Emergent Superstructural Dynamic Order due to Competing Antiferroelectric and Antiferrodistortive Instabilities in Bulk $EuTiO_3$

Jong-Woo Kim,[1,†] Paul Thompson,[2] Simon Brown,[2] Peter S. Normile,[3] John A. Schlueter,[4] Andrey Shkabko,[5] Anke Weidenkaff,[5] and Philip J. Ryan[1,*]

[1]*X-ray Science Division, Argonne National Laboratory, Argonne, Illinois 60439, USA*
[2]*Department of Physics, University of Liverpool, Liverpool L69 3BX, United Kingdom and XMaS, European Synchrotron Radiation Facility, 6 Rue Jules Horowitz, 3800 Grenoble, France*
[3]*Instituto Regional de Investigación Científica Aplicada (IRICA) and Departamento de Física Aplicada, Universidad de Castilla-la Mancha, Spain*
[4]*Materials Science Division, Argonne National Laboratory, Argonne, Illinois 60439, USA*
[5]*Empa, Swiss Federal Laboratories for Materials Science and Technology, Ueberlandstrasse 129, 8600 Duebendorf, Switzerland*
(Received 28 June 2012; published 8 January 2013)

Microscopic structural instabilities of $EuTiO_3$ single crystals were investigated by synchrotron x-ray diffraction. Antiferrodistortive (AFD) oxygen octahedron rotational order was observed alongside Ti derived antiferroelectric distortions. The competition between the two instabilities is reconciled through a cooperatively modulated structure allowing both to coexist. The combination of electric and magnetic fields increases the population of the modulated AFD order, illustrating how the origin of the large magnetoelectric coupling derives from the dynamic equilibrium between AFD and polar instabilities.

DOI: 10.1103/PhysRevLett.110.027201 PACS numbers: 75.85.+t, 61.05.cp, 75.50.Ee, 77.84.Cg

The magnetoelectric (ME) effect involving the cross coupling of the electric and magnetic polarization is an excellent opportunity to study the fundamental physics underlying the interactions of multiple degrees of freedom, including spin (magnetic), polar (electric), and lattice (structure) [1]. Control of the magnetic moment with electric field or electric polarization with magnetic field through the ME effect can also drive new opportunities to develop future applications of low power field sensors, multistate data storage and spintronic devices [2]. Typically, this phenomenon is weak, relegating device application unlikely [1]. However, knowing the mechanism underlying the ME effect will allow one to circumnavigate any factors limiting the coupling strength.

The substantial change of the dielectric constant under an applied magnetic field observed in $EuTiO_3$ indicates a formidable ME coupling in this material [3]. The rare-earth tetravalent titanate $EuTiO_3$ is one of the $ATiO_3$ perovskite members which presents quantum paraelectricity and G-type antiferromagnetic (AFM) order of the Eu sublattice below 5.3 K [4]. Previous theoretical and experimental work predicted and confirmed that strained $EuTiO_3$, in thin film form exhibits ferromagnetic spin alignment as well as spontaneous electric polarization through spin-lattice coupling becoming a strong ferroelectric ferromagnet [5,6]. Recently, evidence of a cubic to tetragonal structural transition was reported, driven supposedly by TiO_6 octahedra rotations, analogous to that observed in $SrTiO_3$ [7,8]. It is well established that antiferrodistortive (AFD) octahedral order competes directly with the electric polarization in tetravalent titanate perovskite systems [9]. These competing instabilities tend to suppress each other so that, generally, one prevails and determines the lowest energy structure. However, the ground state can be modified by external conditions, for example, epitaxial strain or electric field taking advantage of a competitively balanced state [10]. An impressive illustration of this phenomenon was demonstrated by a series of artificial superlattice structures comprised of ferroelectric and paraelectric perovskite oxide components. High dielectric constants were effectively engineered by tuning the competition between these instabilities through multilayer design directly interfacing the competing parameters [11–14].

In this Letter, we present evidence that $EuTiO_3$ naturally forms a superlattice structure reconciling these competitive instabilities. X-ray diffraction data on a single crystal $EuTiO_3$ show a superstructure of AFD TiO_6 octahedral rotations. Furthermore, since the magnetism is strongly coupled with both the electric polarization as well as the oxygen octahedral rotations in this system [15], we have employed *in situ* x-ray diffraction in combined electric and magnetic fields to demonstrate the underlying role oxygen AFD order plays in the ME coupling between the polar Ti and the Eu magnetic moments.

Single crystals of $EuTiO_3$ were grown using a floating-zone furnace equipped with four focused halogen lamps and a flowing mixture of 5% H_2 in Ar. Samples ranged in size between 0.5 and 1 mm^3, displaying high crystallinity with a 0.02° mosaicity. In addition, the requisite magnetodielectric response below T_N was previously published for these samples [16]. X-ray diffraction measurements were performed on the 6ID-B beam line at the Advanced Photon Source and the XMaS beam line at the European Synchrotron Radiation Facility. The sample was mounted

on the cold finger of a Joule-Thomson stage in a closed cycle helium displex refrigerator modified to provide *in situ* high electric field application. The incident x-ray energy was tuned to 16.2 keV for the structural measurement and 7.612 keV, Eu L_{II} edge was used for the x-ray resonant magnetic scattering (XRMS) measurement. The incident x ray is linearly polarized perpendicular to the scattering plane (σ polarization). The resonant magnetic scattering arising from electric dipole ($E1$) transitions from the $2p$-to-$5d$ states, rotates the polarization resulting in π polarized photons (parallel to the scattering plane). Polarization analysis was achieved by using pyrolytic graphite (0 0 6) reflection to select π-polarized magnetic scattering and suppress the background from charge scattering (σ polarized). The sample was thinned down to 400 microns and coated with Au electrodes in order to apply an electric field along the [1 1 0] direction.

Half integer Bragg peaks were observed, arising from AFD octahedral tilting [central reflection in Fig. 1(a)].

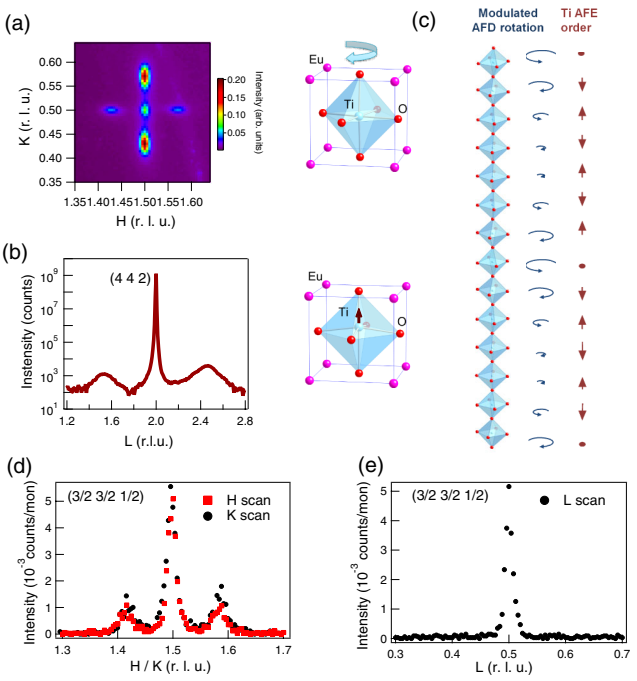

FIG. 1 (color online). (a) Reciprocal space map in H and K of the antiferrodistortive octahedral order reflection at (3/2 1/2 5/2) presenting the modulation satellites and a cartoon depiction illustrating the oxygen octahedral rotations. (b) L scan through the (4 4 2) Bragg reflection and an atomic model of the titanium displacement at 5.2 K. Broad intensity is observed at (4 4 2 $\pm$ 1/2) corresponding to the local AFE order. (c) An atomic model of the modulated AFD order and the corresponding AFE order. The arrows show the possible local electric polarization order but the actual titanium shift direction is not determined from this measurement. (d) H and K scans around (3/2 3/2 1/2). In both scans, the m-AFD reflections are allowed due to H, $K \neq L$ (e) L scan around (3/2 3/2 1/2). The m-AFD reflection is forbidden as $H = K$ at 2 K.

In principle, the symmetry of the octahedral rotation patterns are typically identified by the reflection conditions. It is assumed the system undergoes a structural phase transition from cubic to tetragonal symmetry, $a^0a^0c^-$ in Glazer notation [17,18] similar to $SrTiO_3$ where any a, b, or c axis of the cubic unit cell can become the tetragonal c axis [8]. However, distinguishing a single crystal tetragonal c axis is problematic due to both small lattice changes and a relatively broad mosaicity so that it is inappropriate to apply reflection conditions to identify the symmetry related half order peaks.

Additional scattered intensities, illustrated in Fig. 1(a), are found flanking the half order reflections along H, K and L directions. The wave vector of these peaks is (1/2 1/2 q), (1/2 q 1/2), and (q 1/2 1/2) where $q = \sim 0.43$ indicates an incommensurate superstructure periodicity $\sim$14 unit cells. Fortuitously, the reflection condition for the AFD order states that if two of the H, K, and L are equal, then the satellite reflection is forbidden [Figs. 1(d) and 1(e)]. This indicates that the satellite peaks result from a long range modulation of the AFD octahedral rotation (m-AFD) and that the rotation axis is along the q direction. While oxygen atoms lying on the rotation axis do not change their position by rotation, the other oxygen atoms move from the face center of the perovskite unit cell. Since oxygen atoms share the position with the next unit cell, the wave vector components perpendicular to the rotation axis are constrained to be 1/2. Thus, the underlying character of the AFD order is purely $a^0a^0c^-$ and thus, of the $I4/mcm$ symmetry group. Incidentally, not dissimilar looking satellite modulations were recently identified by electron diffraction [16]. However, their data were inconsistent, given the sensitivity of the technique, this may be a result of irreproducible sample conditions caused by the mechanical grinding of the sintered pelletized $EuTiO_3$ samples. On the other hand, our repeated XRD measurements on several single crystal samples from a series of growth batches have been completely consistent.

Diffuse scattering related to (0 0 1/2) ordering emerges in conjunction with the m-AFD and is attributed to antiferroelectric (AFE) distortions arising from Ti displacements, presented in Fig. 1(b). The associated correlation length of $\sim$6 unit cells is roughly half the length of the m-AFD rotational order. The m-AFD generates regions of both larger and smaller rotation angles of the TiO_6 octahedra. The structure model in Fig. 1(c) illustrates how the short range AFE periodicity forms where the AFD rotations are near a minimum. In order for both AFD and AFE orders to coexist, the competition between them is reconciled through the formation of the super structure where both instabilities are alternatively interwoven.

Additionally, after cooling, the superlattice modulation continues to develop slowly over time. Figure 2(a) shows the evolution of the m-AFD reflection by comparing immediately upon cooling and after 17 hours. The m-AFD peaks

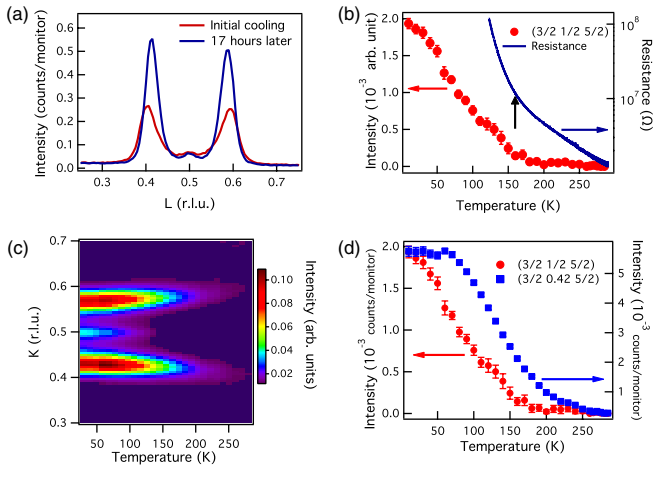

FIG. 2 (color online). (a) The L scans around (7/2 5/2 1/2) right after cooling and 17 hours later. The intensity of the modulated AFD order increases slowly over a long time. (b) The temperature dependence of the AFD intensity at (3/2 1/2 5/2) and the resistance of the sample. The response of resistance variation by temperature changes around 160 K where the AFD order occurs. (c) Temperature dependence of the K scans across (3/2 1/2 5/2) in color scale. (d) The temperature dependence of integrated intensities of normal and modulated AFD order reflections. The normal AFD order disappears around 160 K while the modulated AFD order persists up to 285 K.

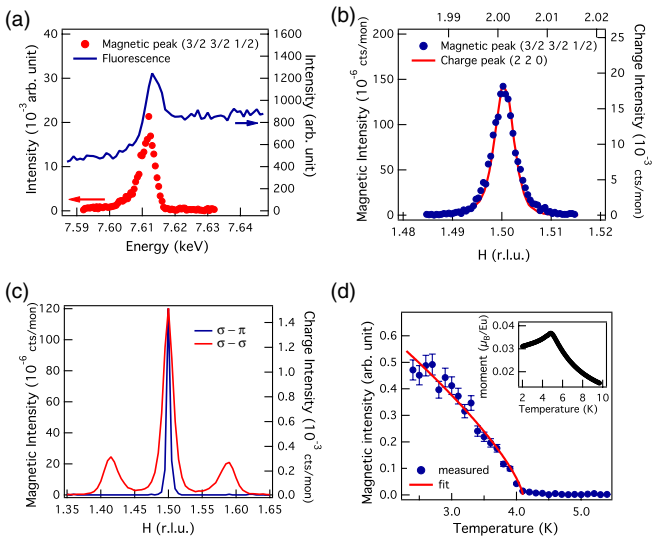

FIG. 3 (color online). (a) Energy scans of the magnetic reflection (3/2 3/2 1/2) in $\sigma - \pi$ geometry and fluorescence. The resonance enhancement is shown at the Eu L_{II} absorption edge. (b) H scans around magnetic reflection (3/2 3/2 1/2) and charge Bragg peak (2 2 0). The width of the magnetic peak is comparable to the width of the charge peak. (c) H scans around (3/2 3/2 1/2) reflection in $\sigma - \sigma$ and $\sigma - \pi$ polarization geometries. Only magnetic intensity from G-type magnetic order is shown in $\sigma - \pi$ geometry while the AFD order reflections are seen in $\sigma - \sigma$ geometries. (d) Temperature dependence of the magnetic intensity and the critical exponent fitting curve. Inset shows the SQUID measurement of magnetization versus temperature curve with 100 Oe.

increase in intensity, shift in position and sharpen over long time periods while the simple AFD intensity remains unchanged. This implies that there is a large relaxation time constant for the modulated structure to form indicating the mediation is a dynamic process with continuing fluctuations between the AFD and AFE order. In contrast, the simple AFD order is static. The correlation lengths of the m-AFD structure are within the nanometer regime, ~11 nm (28 unit cells) and ~22 nm (56 unit cells) parallel and perpendicular to the octahedral rotation axis direction respectively.

The temperature dependence of the K scan across the (3/2 1/2 5/2) reflection is plotted in Figs. 2(c) and 2(d). The m-AFD peak intensity disappears around 285 K, which coincides with a transition found by heat capacity measurements [7]; however, the simple AFD reflection vanishes around ~160 K. Additionally, the incommensurate periodicity contracts with increasing temperature, accelerating as the AFD order dissipates. The resistivity also shows a transition at this temperature shown in Fig. 2(b), which indicates a band gap broadening with static symmetry reduction due to octahedral rotations [19]. In fact, controlling the gap by strain has been calculated in $SrTiO_3$, by changing the degree of oxygen rotation. As a result, the O $2p$ and Ti $3d$ states are more likely to mix and consequently repel each other, essentially driving the respective valence and conduction bands further apart [20].

The presence of G-type antiferromagnetic order at low temperatures was confirmed by x-ray resonant magnetic scattering. Figure 3(a) presents the resonant enhancement of the (3/2 3/2 1/2) magnetic reflection intensity at the Eu L_{II} edge below T_N. Figure 3(b) shows that the width of the magnetic peak along H is comparable to the width of the normal structural Bragg peak indicating the correlation length of magnetic order is comparable to the size of the crystal grain. The clear difference between the AFM and m-AFD correlation lengths demonstrates how the m-AFD order is not associated with crystal quality [Fig. 3(c)]. Both T_N and the critical exponent were extracted from the temperature dependent XRMS intensity in Fig. 3(d), as 4.1 K and 0.373 respectively, showing 3D Heisenberg behavior. The transition temperature measured by XRMS is slightly lower than the SQUID measurement, which is attributed to x-ray beam heating.

The magnetic intensity of AFM ordering as a function of applied B field along the [1 1 1] direction was measured at 2 K and is plotted in Fig. 4. Canting of the magnetic moment occurs along the external magnetic field direction and becomes fully aligned to the field above 0.7 T. The saturation field is lower than the previous measurement on the powder sample (between 1 and 3 T) suggesting that the [1 1 1] direction is the magnetic easy axis. The magnetic response of the m-AFD (7/2 5/2 q) reflection was measured by sweeping the B field along the [1 1 1] direction,

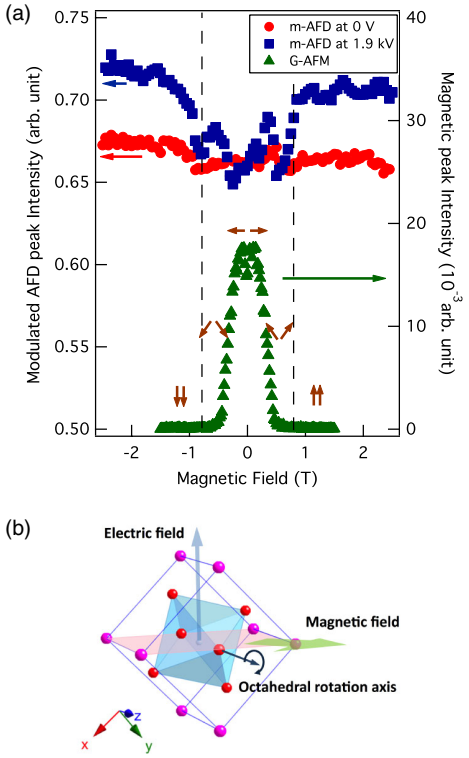

FIG. 4 (color online). (a) The magnetic field effects on the modulated AFD order at (7/2 5/2 q) reflection and AFM order at (3/2 3/2 1/2) magnetic reflection. The red circles represent the intensity of modulated AFD order without E-field application. The blue squares are measurements with E-field, 0.67×10^5 V/cm. A 10% intensity change is shown around the saturation field (~ 0.7 T) with E-field application. The green triangles are intensities of the G-AFM order, which decreases as the magnitude of magnetic field increases and disappears with magnetic moment saturation. The paired arrows show the response of the magnetic moment orientation by external magnetic field. (b) The configuration of the electric and magnetic field directions according to the crystallographic geometry.

with and without applied electric field along the [1 1 0] direction as illustrated in Fig. 4(b).

A small intensity change was observed at the magnetic field saturation points without E-field application. No significant change to the m-AFD reflection is measured with the E field alone and similarly, no effect is observed on the magnetic reflection intensity with the E field either (not shown). Additionally, the magnetic field required to saturate the system remains unchanged with the E field, implying that the maximum E field $\sim 0.67 \times 10^5$ V/cm may not be sufficient to alter the antiferromagnetic interaction [21]. However, a large change of the m-AFD intensity was found when both E and B fields were applied simultaneously. The measurement was made while the E field was fixed at 0.67×10^5 V/cm and the applied B field swept from -2.5 to 2.5 T. A large increase in intensity, up to $\sim 10\%$, is observed through the saturation point, not seen with either E or B field application alone.

This establishes the central role the m-AFD order plays in the underlying mechanism of the magneto-dielectric coupling in this system. As was discussed above, the competition of the octahedral rotation and the electric polarization is accommodated by forming the m-AFD order. It is a dynamic equilibrium state with continuous and coupled fluctuations between the AFD and AFE instabilities. Hence, this delicate balance can be modified by external conditions more readily. It is known that the titanium shift is related to ferromagnetic and antiferromagnetic spin alignment through the spin-lattice coupling [3]. In addition, recent calculations show that the octahedral rotations are indirectly linked to the AFM magnetic interaction energy again through the titanium position [15]. The external electric and magnetic fields alter the dynamically coupled equilibrium state of the AFD and AFE instabilities. As a result, the system responds by shifting to a new equilibrium position and subsequently increases the population of the m-AFD order.

In conclusion, we have revealed a novel dynamic microscopic superstructural response reconciling competing AFD and electric polar instabilities in $EuTiO_3$ single crystals by employing synchrotron x-ray diffraction. Due to the competition between the AFD octahedral rotation and electric polarization, the local structure approaches a dynamic equilibrium state with a large time scale, resulting in a modulated AFD order. By forming this structure, the coexistence of the competing AFD and AFE structural instabilities becomes possible. The equilibrium can be tuned by external electric and magnetic field application, indicating that the m-AFD order is central to the underlying magnetoelectric phenomenon of this system.

Work at Argonne and use of beam line 6-ID-B at the Advanced Photon Source at Argonne was supported by the U.S. Department of Energy, Office of Science, Office of Basic Energy Sciences under Contract No. DE-AC02-06CH11357. The EPSRC-funded XMaS beam line at the ESRF is directed by M. J. Cooper, C. A. Lucas, and T. P. A. Hase. We are grateful to O. Bikondoa, D. Wermeille, and L. Bouchenoire for their invaluable assistance and to S. Beaufoy and J. Kervin for additional XMaS support. Funding for sample growth is provided by SNF NCCR MaNEP. P. J. Ryan acknowledges additional funding from the University of Liverpool and Aer Lingus Group Plc.

*pryan@aps.anl.gov
†jwkim@aps.anl.gov

[1] M. Fiebig, J. Phys. D **38**, R123 (2005).
[2] W. Eerenstein, N. D. Mathur, and J. F. Scott, Nature (London) **442**, 759 (2006).
[3] T. Katsufuji and H. Takagi, Phys. Rev. B **64**, 054415 (2001).
[4] T. R. McGuire, M. W. Shafer, R. J. Joenk, H. A. Alperin, and S. J. Pickart, J. Appl. Phys. **37**, 981 (1966).

[5] C. J. Fennie and K. M. Rabe, Phys. Rev. Lett. **97**, 267602 (2006).
[6] J. H. Lee *et al.*, Nature (London) **466**, 954 (2010).
[7] A. Bussmann-Holder, J. Kohler, R. K. Kremer, and J. M. Law, Phys. Rev. B **83**, 212102 (2011).
[8] M. Allieta, M. Scavini, L. J. Spalek, V. Scagnoli, H. C. Walker, C. Panagopoulos, S. S. Saxena, T. Katsufuji, and C. Mazzoli, Phys. Rev. B **85**, 184107 (2012).
[9] W. Zhong and D. Vanderbilt, Phys. Rev. Lett. **74**, 2587 (1995).
[10] D. G. Schlom, L.-Q. Chen, C.-B. Eom, K. M. Rabe, S. K. Streiffer, and J.-M. Triscone, Annu. Rev. Mater. Res. **37**, 589 (2007).
[11] E. Bousquet, M. Dawber, N. Stucki, C. Lichtensteiger, P. Hermet, S. Gariglio, J.-M. Triscone, and P. Ghosez, Nature (London) **452**, 732 (2008).
[12] P. Zubko, N. Stucki, C. Lichtensteiger, and J.-M. Triscone, Phys. Rev. Lett. **104**, 187601 (2010).
[13] X. Wu, K. M. Rabe, and D. Vanderbilt, Phys. Rev. B **83**, 020104(R) (2011).
[14] P. Aguado-Puente, P. Garcia-Fernandez, and J. Junquera, Phys. Rev. Lett. **107**, 217601 (2011).
[15] P. J. Ryan *et al.*, Nat. Commun. **4**, 1334 (2013).
[16] V. Goian, S. Kamba, O. Pacherova, J. Drahokoupil, L. Palatinus, M. Dusek, J. Rohlicek, M. Savinov, F. Laufek, W. Schranz, A. Fuith, M. Kachlik, K. Maca, A. Shkabko, L. Sagarna, A. Weidenkaff, and A. A. Belik, Phys. Rev. B **86**, 054112 (2012).
[17] A. M. Glazer, Acta Crystallogr. Sect. B **28**, 3384 (1972).
[18] K. Z. Rushchanskii, N. A. Spaldin, and M. Lezaic, Phys. Rev. B **85**, 104109 (2012).
[19] H. W. Eng, P. W. Barnes, B. M. Auer, and P. M. Woodward, J. Solid State Chem. **175**, 94 (2003).
[20] R. F. Berger, C. J. Fennie, and J. B. Neaton, Phys. Rev. Lett. **107**, 146804 (2011).
[21] The antiferromagnetic interaction is determined by the third nearest neighbor Eu ion mediated by a superexchange interaction via Eu-Ti-Eu. Displacing the Ti atom by external electric field should alter the balance of antiferromagnetic and ferromagnetic interaction preferentially suppressing the antiferromagnetic interaction [15].